MATERIALS SCIENCE

Integrated textile sensor patch for real-time and multiplex sweat analysis

Wenya He[1,2], Chunya Wang[1], Huimin Wang[1], Muqiang Jian[1], Wangdong Lu[1], Xiaoping Liang[1], Xin Zhang[2], Fengchun Yang[2]*, Yingying Zhang[1]*

Copyright © 2019 The Authors, some rights reserved; exclusive licensee American Association for the Advancement of Science. No claim to original U.S. Government Works. Distributed under a Creative Commons Attribution NonCommercial License 4.0 (CC BY-NC).

Wearable sweat analysis devices for monitoring of multiple health-related biomarkers with high sensitivity are highly desired for noninvasive and real-time monitoring of human health. Here, we report a flexible sweat analysis patch based on a silk fabric–derived carbon textile for simultaneous detection of six health-related biomarkers. The intrinsically N-doped graphitic structure and the hierarchical woven, porous structure provided the carbon textile good electrical conductivity, rich active sites, and good water wettability for efficient electron transmission and abundant access to reactants, enabling it to serve as an excellent working electrode in electrochemical sensors. On the basis of the above, we fabricated a multiplex sweat analysis patch that is capable of simultaneous detection of glucose, lactate, ascorbic acid, uric acid, Na^+, and K^+. The integration of selective detectors with signal collection and transmission components in this device has enabled us to realize real-time analysis of sweat.

INTRODUCTION

With the development of portable healthcare systems, real-time monitoring of health-related multiple biomarkers has attracted attention. Conventional medical detection of biomarkers, which generally require blood samples and cumbersome instruments, is invasive and time consuming and requires professional technique. By contrast, flexible sensors for biomarkers hold great promise for personalized healthcare devices owing to their combined features of less/noninvasive manner and real-time monitoring (*1*–*5*). In addition to blood samples, sweat contains various health-related biomarkers including biomolecules [e.g., ascorbic acid (AA) and uric acid (UA)], metabolites (e.g., glucose and lactate), and electrolytes (e.g., Na^+ and K^+) and thus has been chosen for noninvasively assessing individual's physiological state by detecting biomarkers in sweat (*6*, *7*). Pioneer researchers have developed various noninvasive and flexible sensors for sweat analysis, including colorimetric sensors (*8*–*10*), electrochemical sensors (*11*–*13*), and fluorescence sensors (*14*, *15*). The electrochemical method is the most popular way owing to advantages of relatively high sensitivity and selectivity, rapid response, as well as good compatibility (*16*–*19*). However, wearable electrochemical sweat analysis devices still confront notable challenges, such as relatively low sensitivity and selectivity in simultaneous measurement of multiple biomarkers as well as complexity in fabrication procedure.

The rational design of working electrode materials is the key for the sensing performance of wearable electrochemical sensors. Various materials have been used as working electrodes, such as noble metal (Au and Ag) (*20*–*22*), metallic oxides (*23*, *24*), graphene (*25*, *26*), and carbon black (*27*). However, these materials have limitations, such as poor stability, inferior electrical conductivity, and limited flexibility and wettability, which emphasize the urgency of developing new and promising electrode materials. Silk, an ancient natural fiber, has been used for the fabrication of soft and breathable fabrics with large-scale production for thousands of years (*28*, *29*). Compared to other animal fibers (e.g., wool), an obvious advantage of silkworm silk fibers is its large length up to 1.5 km, endowing silk fabric with good uniformity and high mechanical strength. Recently, it has been reported that silk fabrics can be transformed into highly conductive, intrinsically nitrogen-doped, flexible, and structure-maintained carbon textiles through thermal treatment (*30*–*35*). Compared with the common electrode materials, the flexible silk-derived carbon textiles show intrinsic hierarchical and porous mesh woven structure, facilitating good contact with reactants and efficient electron transfer. These unique features endow the silk-derived carbon textile with great potential to serve as the working electrode of wearable electrochemical sensor.

On the basis of silk fabric–derived intrinsically nitrogen (N)–doped carbon textile (SilkNCT), we have developed a flexible, wearable patch for real-time, multiplex sweat analysis. SilkNCT, with high electrical conductivity owing to its intrinsically N-doped graphitic nanocarbon structure, as well as the hierarchical woven, porous structure, was directly used or combined with other compounds to serve as the working electrode of the wearable electrochemical sensor. A facile, cost-effective laser processing strategy was used to fabricate the SilkNCT-based electrochemical sensor array. The flexible patch with the integrated SilkNCT-based sensor array could simultaneously detect six biomarkers (glucose, lactate, AA, UA, Na^+, and K^+) with high sensitivity, good selectivity, and long-term stability. Furthermore, the sweat analysis patch was integrated with signal collection and transmission circuit components, realizing the on-body, real-time monitoring of multiple biomarkers in sweat. As a proof of concept, the smart sweat patch was used to monitor the glucose concentration in a volunteer's perspiration, and the results were comparable with commercial high-performance liquid chromatography–mass spectrometry (HPLC-MS). This work provides a promising strategy for the fabrication of wearable, multiplex sweat analysis devices.

RESULTS

Design and fabrication of wearable sweat analysis patch

Figure 1A illustrates the SilkNCT-based wearable, multiplex sensor patch, which can be mounted on human skin for in situ sweat analysis. Six electrochemical sensors are integrated into the flexible patch

[1]Key Laboratory of Organic Optoelectronics and Molecular Engineering of the Ministry of Education, Department of Chemistry, Tsinghua University, Beijing 100084, China. [2]Key Laboratory of Synthetic and Natural Functional Molecule Chemistry of Ministry of Education, College of Chemistry and Materials Science, Northwest University, Xi'an, 710127, China.
*Corresponding author. Email: yingyingzhang@tsinghua.edu.cn (Y.Z.); fyang@nwu.edu.cn (F.Y.)

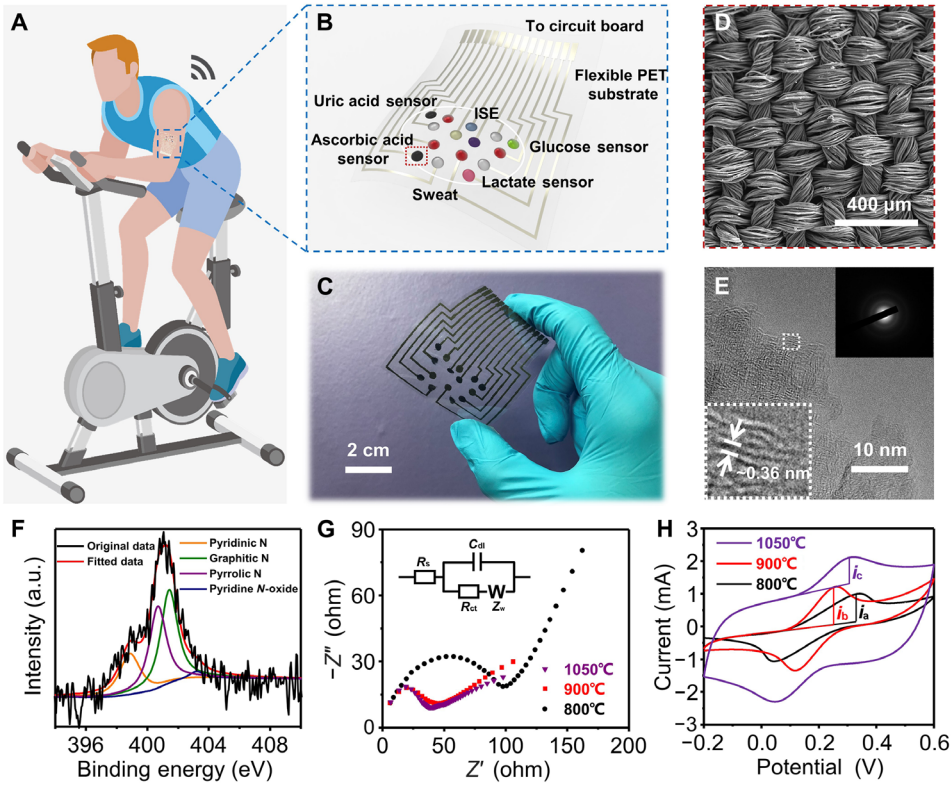

Fig. 1. Wearable sweat analysis patch based on SilkNCT. (**A** and **B**) Schematic illustration of wearable sweat analysis patch mounted on human skin (A) and the multiplex electrochemical sensor array integrated in the patch (B). (**C**) Photograph of the wearable sweat analysis patch. (**D** and **E**) SEM (D) and TEM (E) images of the carbonized silk fabric, showing its hierarchical woven macrostructure and microcrystalline graphite-like microstructure, respectively. (**F**) High-resolution XPS spectrum of N1s for the carbonized silk fabric. a.u., arbitrary units. (**G**) EIS of the carbonized silk fabric prepared at different temperatures. Inset in (G) shows an equivalent circuit model. (**H**) Cyclic voltammograms of the carbonized silk fabric prepared at different temperatures in 0.1 M KCl solution containing 5.0 mM $[Fe(CN)_6]^{3-/4-}$. Photo credit: Wenya He, Tsinghua University.

(Fig. 1B), allowing simultaneous detection of six health-related biomarkers (glucose, lactate, AA, UA, Na^+, and K^+). SilkNCT was directly used or combined with other compounds to serve as the working electrodes of the flexible electrochemical sensors. The circuit was fabricated from a conductive Ni-coated textile tape using a facile digital laser writing technique (see fig. S1 for the detailed fabrication process of the sweat analysis patch). Figure 1C shows the photograph of the flexible patch, which can be conformably mounted on human body for in situ sweat analysis.

Morphology and structure of SilkNCT

The hierarchical and porous structure as well as graphitic nanocarbon structure endow SilkNCT with good flexibility, more access to reactants, and high electrical conductivity, making SilkNCT promising for applications as the working electrodes of electrochemical sensors. Figure 1D shows the scanning electron microscopy (SEM) image of SilkNCT. SilkNCT has well-reserved woven structures inherited from the pristine silk fabric, in which the weft yarns are composed of parallel fibers and the warp yarns are composed of twisted fibers. The unique woven structure endows SilkNCT with hierarchical and porous structure, benefiting to the efficient electron transmission and abundant access to reactants. Transmission electron microscopy (TEM) image of SilkNCT, as shown in Fig. 1E, displays the distorted lattice fringes with an interlayer spacing of ~0.36 nm, which belongs to the interplanar spacing of the (002) plane for hexagonal graphite (*36*), indicating the graphitic nanocarbon structure of SilkNCT. Note that as-obtained SilkNCT has good water wettability (fig. S2), which contributes to the quick diffusion of electrolyte, and, accordingly, the efficient electrochemical reaction on the SilkNCT electrode.

X-ray photoelectron spectroscopy (XPS) reveals the chemical composition of SilkNCT. The contents of C, N, and O elements are 81.25, 3.3, and 15.45%, respectively. In comparison, the pristine silk fabric is composed of C, N, and O elements with the contents of 51.79, 28.87, and 18.51%, respectively (see fig. S3A and table S1). Figure 1F shows that the N1s spectrum could be fitted by four peaks attributed to the pyridinic N, pyrrolic N, quaternary or graphitic N, and pyridine *N*-oxide N, respectively, indicating that part of N elements in pristine silk has transformed into N substituents in graphitic carbon (*34*, *35*, *37*). The C1s spectrum also confirms the presence of the C-N structure (fig. S3B). The sp^2-hybridized hexagonal carbon structure and the intrinsic doping of N provide SilkNCT with good electrical conductivity and abundant active sites, which are beneficial for SilkNCT as efficient electrochemical electrode materials.

Electrochemical activity of SilkNCT

The carbonization temperature was optimized to obtain SilkNCT with low charge-transfer resistance and high electrochemical activity. The *I*-*V* curves of SilkNCT prepared with different carbonization temperatures (800°, 900°, and 1050°C) show that SilkNCT with higher carbonization temperature had higher electrical conductivity (fig. S4), which could be attributed to the fact that higher temperature leads to enhanced graphitization degree. Furthermore, electrochemical

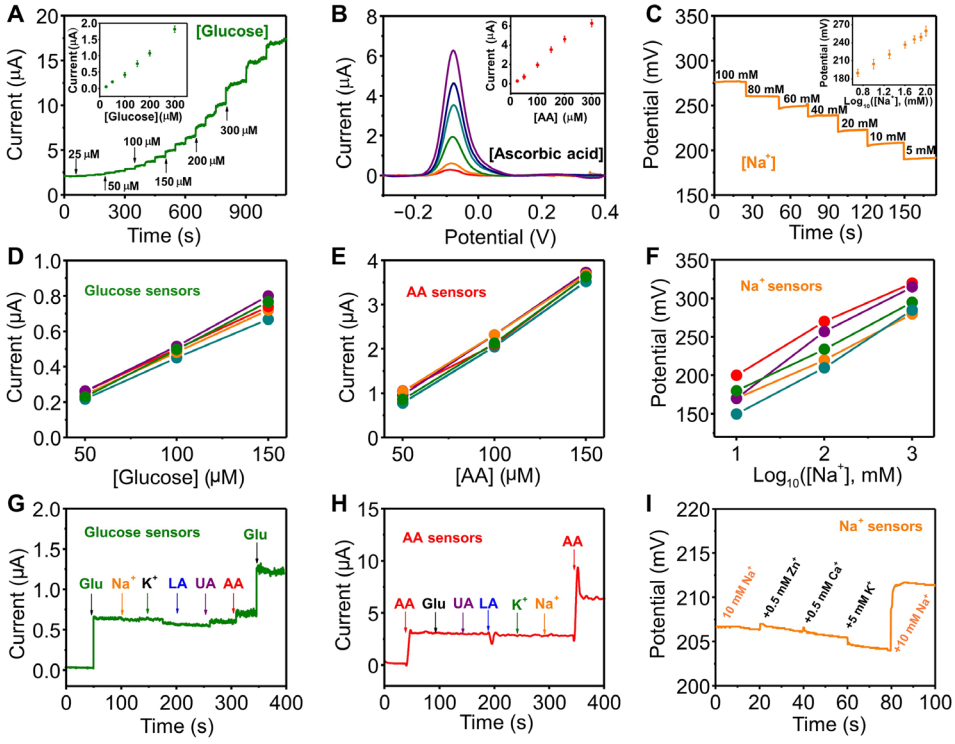

Fig. 2. Performance of the flexible SilkNCT-based sensors for multiple biomarkers. (**A**) Chronoamperometry responses of the SilkNCT-based glucose sensor. (**B**) DPV responses of the SilkNCT-based AA sensor to the AA solution in phosphate-buffered saline (PBS). (**C**) OCP responses of the SilkNCT-based Na^+ sensor. Insets in (A) to (C) show the corresponding calibration plots of the sensors. The error bars represent the SDs of the measured data with five points. (**D** to **F**) Reproducibility of the SilkNCT-based glucose sensors (D), AA sensors (E), and Na^+ sensors (F). (**G** to **I**) Selectivity of the SilkNCT-based glucose sensors (G), AA sensors (H), and Na^+ sensors (I).

impedance spectroscopy (EIS) was used to characterize the charge-transfer resistance. Figure 1G exhibits the EIS curves of SilkNCT prepared with different temperatures. The inset of Fig. 1G shows an equivalent circuit model, which includes the ohmic resistance of the electrolyte (R_s), the Warburg impedance (Z_w), the charge-transfer resistance (R_{ct}), and an interfacial capacitance (C_{dl}). The EIS curves consist of a semicircle part corresponding to charge-transfer resistance and a straight line part corresponding to the diffusion process. The smaller semicircle of the curves for SilkNCT obtained at 900° and 1050°C indicate the lower R_{ct} of the corresponding SilkNCT than that obtained at 800°C. Therefore, the electron transfer rate is higher when using the SilkNCT electrode fabricated at higher temperature. Cyclic voltammetry (CV) was performed to measure the electrochemical activity of SilkNCT. CV curves in Fig. 1H show the electrochemical activity of SilkNCT using $[Fe(CN)_6]^{4-}/[Fe(CN)_6]^{3-}$ redox couple as an electrochemical probe, revealing that SilkNCT obtained at 900°C displayed the highest Faraday current. Because higher faraday current is derived from redox reaction on the SilkNCT electrode, the results indicate that SilkNCT obtained at 900°C had the highest electrochemical activity. We analyzed the gross content of N and the relative content of different N species in SilkNCT obtained at different temperatures (fig. S5 and table S2). Compared to SilkNCT obtained at 1050°C, SilkNCT obtained at 900°C contains obviously more N, where most of the N is active pyridinic N and graphitic N, which are proved to contribute to high activity toward electrochemical reaction (*38*, *39*). The synergistic effect of the above factors endows SilkNCT obtained at 900°C with lower charge-transfer resistance and higher electrochemical activity than that obtained at other temperatures, making it preferable for serving as the working electrode of electrochemical sensors. Besides, we also compared the performance of SilkNCT with carbonized cotton fabric (fig. S6). The results show that carbonized cotton fabric has obviously worse sensing performance than SilkNCT, which may be ascribed to the fact that it lacks N. The following results are all based on SilkNCT obtained at 900°C except otherwise indicated.

Fabrication and performance of SilkNCT-based electrochemical sensors

On the basis of SilkNCT, various electrochemical sensors, including two enzyme-based amperometric sensors for glucose and lactate, two amperometric sensors for AA and UA, and two ion-selective sensors for Na^+ and K^+, were designed and fabricated (see fig. S7 for the working mechanism of each sensors). For the AA and UA sensors, pristine SilkNCT, based on its good electrical conductivity and abundant active sites, was directly used as the working electrode. An oxidation reaction will occur on the SilkNCT electrode when it makes contact with AA or UA. There are abundant active sites on the N-doped SilkNCT, facilitating the electron transfer. For the fabrication of enzyme-based amperometric sensors, SilkNCT was first equipped with homogeneously distributed Pt nanospheres (fig. S8, A to D) to achieve high sensitivity. Next, glucose oxidase and lactate oxidase were evenly loaded on SilkNCT to realize the selective detection of glucose or lactate (fig. S8, E and F). For the detection of glucose or lactate, the functionalized SilkNCT serves as the working electrode, which can respond to hydrogen peroxide. Note that hydrogen peroxide is a by-product of the enzymatic oxidation of glucose or lactate. The good electrical conductivity, rich active sites derived from N-doping, and the hierarchical woven, porous structure of SilkNCT enable it to serve as an excellent working electrode for achieving

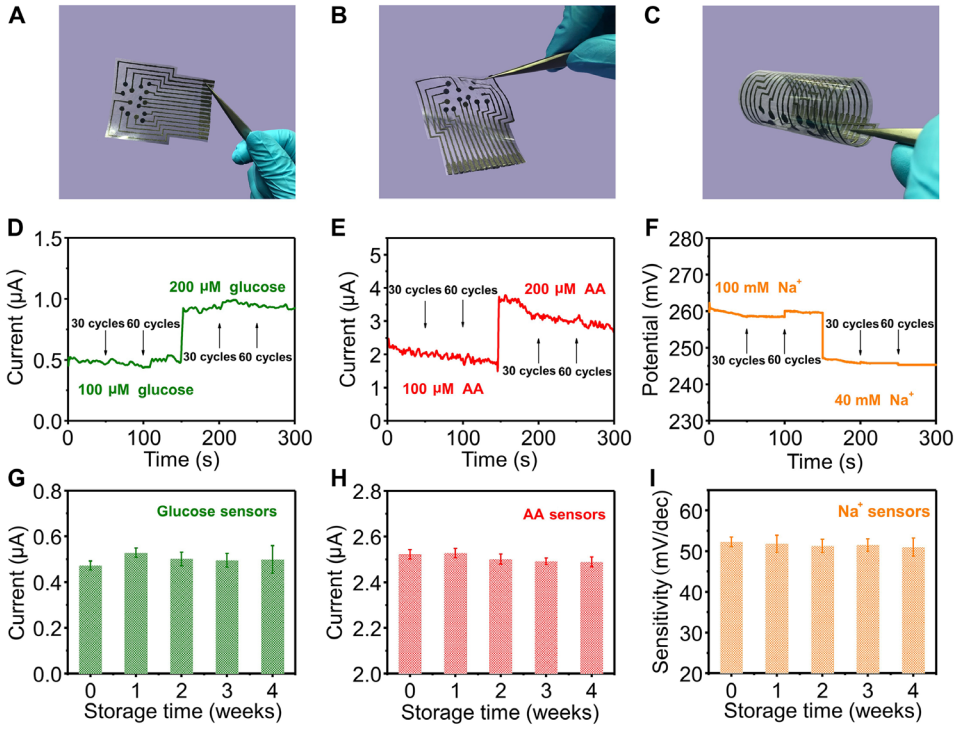

Fig. 3. Flexibility and stability of the SilkNCT-based flexible electrochemical sensors. (**A** to **C**) Photographs of the as-prepared SilkNCT-based flexible sensor array. (**D** to **F**) Electrochemical responses of the SilkNCT-based glucose sensors (D), AA sensors (E), and Na^+ sensors (F) after different bending cycles. Data recording was paused for bending cycles in (D) to (F). (**G** to **I**) Electrochemical responses of the SilkNCT-based glucose sensors (G), AA sensors (H), and Na^+ sensors (I) after different storage time. The error bars represent the SDs of the measured data from five samples. Photo credit: Wenya He, Tsinghua University.

high sensitivity. For the fabrication of ion-selective sensors, SilkNCT was combined with poly(3,4-ethylenedioxythiophene) poly(styrenesulfonate) (PEDOT:PSS) as the ion-electron transducer and uniform and transparent ion-selective membranes to improve selectivity (fig. S9, A to C). Hierarchical woven, porous structure and good water wettability endow the textile electrode for quick diffusion of electrolyte and efficient ion and electron transmission.

The SilkNCT-based electrochemical sensors show high sensitivity for detecting multiple analytes (Fig. 2). Figure 2A exhibits the current responses of the SilkNCT-based glucose enzyme sensor to glucose. The inset of Fig. 2A shows that the currents were linearly proportional to glucose concentrations in the range of 25 to 300 μM, from which the sensitivity could be calculated to be 6.3 nA μM^{-1}. The limit of detection (LOD) of the glucose sensor was 5 μM. The lactate sensor exhibited a linear range of 5 to 35 mM and an LOD of 0.5 mM with a sensitivity of 174.0 nA mM^{-1} (fig. S10A). For AA and UA, differential pulse voltammetry (DPV) was used to detect such small biomolecules. Figure 2B shows representative oxidation peaks of AA, and the currents increased linearly with increased AA concentrations. In particular, the SilkNCT-based AA sensor showed a linear range of 20 to 300 μM with an LOD of 1 μM and a sensitivity of 22.7 nA μM^{-1}. Similarly, the SilkNCT-based UA sensor showed a linear range of 2.5 to 115 μM with a sensitivity of 196.6 nA μM^{-1} (fig. S10B). The LOD for the UA sensor was 0.1 μM. The high sensitivity of the AA and UA sensors made of pristine SilkNCT can be attributed to the N-doping and the hierarchical structure of SilkNCT, which promote the electrochemical activity for redox reactions of the molecules. The SilkNCT-based Na^+ and K^+ sensors showed linearly increased open circuit potential (OCP) with concentrations of 5 to 100 mM for Na^+ (Fig. 2C) and 1.25 to 40 mM for K^+ (fig. S10C), corresponding to sensitivity of 51.8 and 31.8 mV per decade of concentration for Na^+ and K^+, respectively. The LODs of the Na^+ and K^+ sensors were 1 and 0.5 mM, respectively. The above results show that all six kinds of SilkNCT-based electrochemical sensors have competitive sensitivity compared with reported work (table S3), indicating its potential for efficient detection of the biomarkers in sweat analysis.

The SilkNCT-based sensors also showed good reproducibility and selectivity, which are important for practical applications. Figure 2 (D to F) (and fig. S10, D to F) shows that the SilkNCT-based sensors fabricated in different batches exhibited similar responses. The relative standard deviations (RSDs) are 3.6% for glucose, 4.2% for lactate, 2.8% for AA, 3.9% for UA, 8.2% for Na^+, and 7.5% for K^+, demonstrating the good reproducibility of these sensors. It is prerequisite that each sensor has a good selectivity to a certain targeted biomarker to integrate them into a versatile sensing patch. The selectivity of the SilkNCT-based sensors was carefully investigated (Fig. 2, G to I, and fig. S10, G to I). Compared with the signal of the targeted molecule, no noticeable interference signals were detected, implying the good selectivity of each sensor, which is beneficial to the construction of a multiplex sensing system.

In addition, flexibility and long-term stability are also of great importance for wearable sensors. Owing to the intrinsic flexibility of SilkNCT and the textile circuit, the integrated sensing patch showed good flexibility. Figure 3 (A to C) shows that the patch mounted on polyethylene terephthalate (PET) can be folded and scrolled while keeping its structural integrity, showing good flexibility. Besides, we also fabricated a sensing patch on a common silk fabric to demonstrate

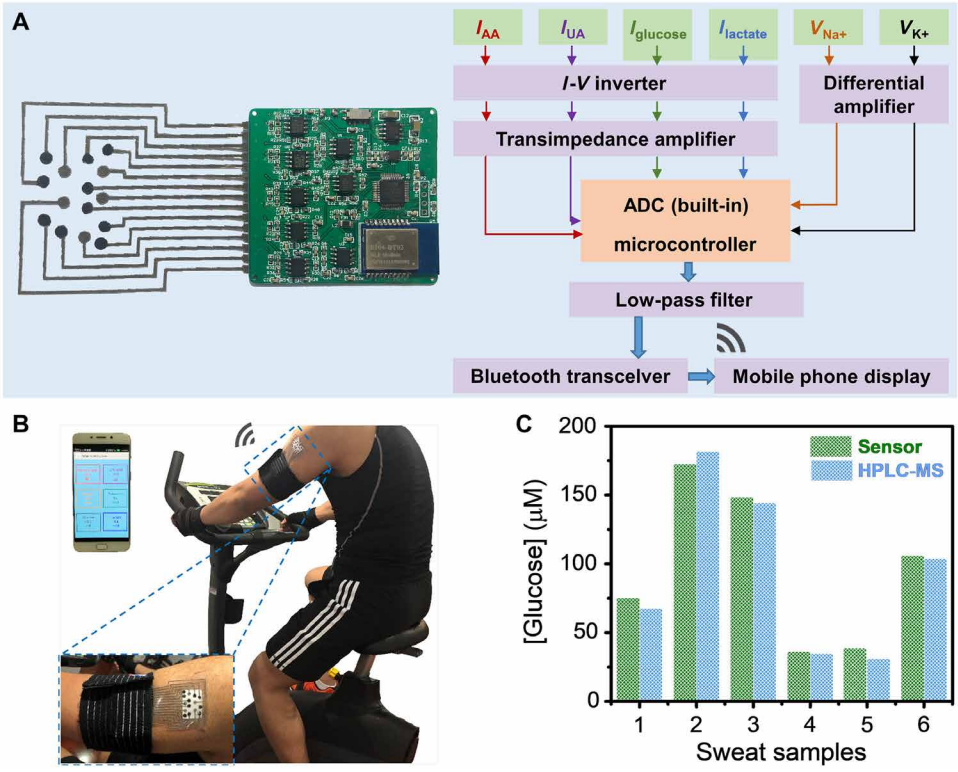

Fig. 4. The integrated sweat analysis patch and its application for real-time and wireless sweat analysis. (**A**) Photograph and illustration of the integrated sweat analysis patch composed of six sensors, signal collection/transduction/conditioning/processing, and wireless transmission components. (**B**) Photograph showing the sweat analysis patch mounted on the arm of a volunteer (in physical activity) for in situ monitoring of the biomarkers in his sweat. (**C**) Comparison of the glucose concentrations detected by the sweat analysis patch and HPLC-MS. Photo credit: Wenya He, Tsinghua University.

the flexibility of the whole system for wearing purposes (fig. S11). We tracked the performance of each sensor after bending deformation. The responses of sensors showed no significant change after different bending cycles, further demonstrating good flexibility (Fig. 3, D to F, and fig. S12, A to C). In addition, the electrochemical responses of the SilkNCT-based sensors showed negligible changes over 4 weeks (Fig. 3, G to I, and fig. S12, D to F), with RSDs of 6.4% for glucose, 5.4% for lactate, 0.8% for AA, 3.4% for UA, 2.9% for Na^+, and 1.8% for K^+. The results revealed the long-term stability of the SilkNCT-based sensors, which could be attributed to the good stability of the graphitic nanocarbon structure of SilkNCT.

Integrated sensing patch for wireless, on-body, and real-time sweat analysis

Furthermore, the flexible, multiplex sensing patch was integrated with a signal collection and transmission circuit component to work as a wireless, on-body, and real-time sweat analysis patch. Figure 4A shows that the multiplex sensor array was connected with a component for signal collection and transmission. Figure 4A also illustrates the integrated system with different functional parts, including signal transduction, conditioning, processing, and wireless transmission from sensors to a mobile phone. As a proof of concept, we used a wristband to fix the integrated patch on the arm of a volunteer and showed its performance for real-time sweat analysis. Figure 4B shows that the biomarkers in the sweat of the volunteer (in physical activity) can be tracked in real time by the sweat analysis patch, and the results could be displayed by a smartphone. Besides, we have compared the results regarding the glucose concentration in the volunteer's sweat obtained by the sweat analysis patch and a highly reliable HPLC-MS approach. The results of our sweat analysis patch are consistent with those from HPLC-MS (Fig. 4C), indicating good reliability and great potential of the wearable sweat analysis patch for noninvasive human health monitoring.

DISCUSSION

In summary, on the basis of SilkNCT, we developed a flexible, multiplex sweat analysis patch with high sensitivity, good selectivity, long-term stability, and good repeatability for monitoring of six health-related biomarkers (glucose, lactate, AA, UA, Na^+, and K^+). The intrinsically N-doped graphitic nanocarbon structure and the hierarchical woven, porous structure provided SilkNCT with good electrical conductivity and much access to reactants as well as facilitated electron transmission. These merits endow SilkNCT with great potential for serving as the working electrode of electrochemical sensors. On the basis of the superior performance of each of the SilkNCT-based electrochemical sensor, a flexible, multiplex sweat analysis patch was fabricated. Furthermore, the sweat analysis patch was integrated with signal collection and transmission components, realizing real-time monitoring of biomarkers in sweat. As a proof of concept, we demonstrated the on-body, wireless monitoring of the biomarkers in the sweat of a volunteer in physical exercise. The versatility, high sensitivity, and

remarkable stability of the sweat analysis patch, along with its facile fabrication process, hold promising practical applications in real-time monitoring of human health.

MATERIALS AND METHODS

Materials

Selectophore grade sodium ionophore X, bis(2-ethylehexyl) sebacate (DOS), sodium tetrakis[3,5-bis(trifluoromethyl)phenyl]borate (Na-TFPB), high–molecular weight polyvinyl chloride (PVC), tetrahydrofuran, valinomycin (potassium ionophore), sodium tetraphenylborate (NaTPB), cyclohexanone, polyvinyl butyral resin BUTVAR B-98 (PVB), 3,4-ethoxylenedioxythiophene (EDOT), NaPSS, glucose oxidase (from *Aspergillus niger*), L-lactate oxidase (>80 activity units/mg), AA, UA, lactate, and glucose were purchased from J&K Scientific. Chitosan, acetic acid, disodium hydrogen phosphate (Na_2HPO_4), potassium dihydrogen phosphate (KH_2PO_4), sodium chloride (NaCl), potassium chloride (KCl), potassium ferricyanide (III), and potassium ferricyanide (II) were obtained from Sigma-Aldrich. All other chemicals (analytical reagent grade) were commercially available and used without further purification. All solutions were prepared using deionized water (18.3 megohm·cm) produced from a Millipore water purification system.

Carbonization of silk fabric

The fabrics were carbonized under a mixed atmosphere of argon [purity, 99.999%; gas flow, 110 standard cubic centimeters per minute (sccm)] and hydrogen (purity, 99.999%; gas flow, 10 sccm) in a tube furnace with the following heat treatment programming: (i) being heated from 25° to 120°C within 10 min and kept for 30 min; (ii) being heated to 350°C at a rate of 5°C min^{-1} and kept for 150 min; (iii) being heated to 900°C (800° and 1050°C) at a rate of 3°C min^{-1} and kept for 90 min; and (iv) naturally cooling down to room temperature.

Characterization

The morphology, structure, and composition of SilkNCT were investigated by SEM [field-emission (FE)–SEM, FEI Quanta 650], TEM (FE-TEM, JEOL JEM2010F), and XPS (Thermo Scientific ESCALAB 250Xi, Al K_α radiation), respectively. Electrochemical measurements, CV, DPV, *i-t* curve, chronoamperometry, OCP, and EIS (with AC impedance) measurements were carried out with a CHI760E workstation (CH Instruments Inc.). In contrast, the collected sweat samples were also determined using HPLC-MS (Thermo Q Exactive).

Fabrication of the SilkNCT-based electrochemical sensor array

First, a nickel conductive tape was used to fabricate well-designed flexible conductive path through a facile digital laser processing technique. SilkNCT was clipped into small round pieces. Then, the flexible conductive path was transferred onto a flexible PET substrate. Traditional three-electrode configuration was constructed for amperometric sensors with the clipped SilkNCT (obtained at 900°C) pieces for working electrodes, SilkNCT (obtained at 1050°C) pieces as counter electrodes, and the Ag/AgCl ink–modified conductive tape as reference electrodes. SilkNCT obtained at 1050°C was selected as the counter electrode due to its relatively higher electrical conductivity compared with SilkNCT obtained at lower temperature. The two-electrode system, with the small SilkNCT (obtained at 900°C) piece as the working electrode and Ag/AgCl as the reference electrode, was designed for ion-selective sensors. Considering the low concentration of biomarkers in sweat, we designed the final electrode with a diameter of 3 mm to obtain a high current. After the sensor array design was finished, Ecoflex was used as an insulating layer to prevent the possible electrical contact of the conductive path with skin and sweat.

Fabrication of lactate and glucose sensors

To prepare the enzyme-based sensors, target oxidase solution was prepared in advance and stored at 4°C for 6 hours. Glucose oxidase solution was prepared by dissolving glucose oxidase powders in phosphate-buffered saline (PBS) with pH 7.2 (10 mg ml^{-1}). Then, the prepared glucose oxidase solution was mixed thoroughly with chitosan solution (1% chitosan in 2% acetic acid) in a volume ratio of 1:1. Lactate oxidase solution with a concentration of 40 mg ml^{-1} was also prepared by dissolving lactate oxidase powders in PBS. To prepare the working electrodes of enzyme-based sensors, an electrochemical deposition process was performed in a solution of 5 mM H_2PtCl_6 and 0.1 M HCl at −0.1 V for 5 min to obtain the Pt nanosphere–decorated SilkNCT (Pt/SilkNCT). The final working electrode of the glucose sensor was fabricated by drop-casting 10 μl of the glucose oxidase/chitosan solution onto the Pt/SilkNCT electrode. For the lactate sensors, Pt/SilkNCT was covered with 5 μl of lactate oxidase solution and 5 μl of chitosan solution.

Fabrication of Na^+ and K^+ selective sensors

First, selective membrane solution and PVB reference electrode solution were prepared according to the methods in the reported literature (*40*). The Na^+ selective membrane was composed of Na ionophore X (1%, w/w), Na-TFPB (0.55%, w/w), PVC (33%, w/w), and DOS (65.45%, w/w). Then, 400 mg of the mixture was dissolved in 2640 μl of tetrahydrofuran with stirring for 30 min. Similarly, K^+ selective membrane cocktail, which consisted of valinomycin (2%, w/w), NaTPB (0.5%), PVC (32.7%, w/w), and DOS (64.7%, w/w), was dissolved in cyclohexanone to get membrane solution. The ion-selective solutions were sealed and stored at 4°C. PEDOT:PSS was used as the ion-electron transducer to minimize the potential drift of the ion-selected electrode (ISE) and was deposited onto the working electrodes by galvanostatic electrochemical polymerization from a solution containing 0.01 M EDOT and 0.1 M NaPSS. Ion-selective membranes were then prepared by drop-casting 10 μl of Na^+ selective membrane solution and 4 μl of K^+ selective membrane solution onto their corresponding electrodes. The PVB reference solution was prepared by dissolving 79.1 mg of PVB and 50 mg of NaCl into 1 ml of methanol with stirring for 1 hour. Then, the reference electrodes for ISEs were fabricated by casting 10 μl of PVB reference solution onto the Ag/AgCl electrodes.

Electrochemical measurements

The electrochemical characterization of the flexible sensor was evaluated in a 0.1 M PBS (pH 7.0) with change concentration of analyst. The AA and UA sensors were evaluated by DPV with oxidation of −0.08 V (versus Ag/AgCl) for AA and 0.21 V (versus Ag/AgCl) for UA. Chronoamperometry was used for the determination of lactate and glucose with an initial potential of −0.2 V (versus Ag/AgCl) for lactate and 0.65 V (versus Ag/AgCl) for glucose, respectively. As for Na^+ and K^+ sensors, direct recording of OCP from the two-electrode system was used. The LOD was defined as the lower concentration

in which the response was three times the SD of noise. To investigate the reproducibility of the sensors, the electrochemical responses of five samples fabricated in different batches were compared. To investigate the stability of the sensors, the performance of five samples were recorded each week over a period of 4 weeks, and other times, the samples were stored at 4°C to preserve the activity of the enzyme on the sensor.

On-body sweat analysis

On-body evaluation of analyst in sweat was performed in five healthy subjects, aged 20 to 30 years. For real-time glucose monitoring, the wristband was connected to the smartphone app via Bluetooth. Volunteers were asked to wear the wristband and cycled for half an hour. The test button was then pressed down to initiate the analysis, and results were displayed on the screen of smartphone after completion of the analysis. Sweat was simultaneously collected to compare sensor data with measurements from HPLC-MS.

SUPPLEMENTARY MATERIALS

Supplementary material for this article is available at http://advances.sciencemag.org/cgi/content/full/5/11/eaax0649/DC1

Fig. S1. Schematic illustration of the fabrication process of the flexible multiple electrochemical sensor array.
Fig. S2. Hydrophilic characterization of carbonized silk fabric.
Fig. S3. XPS survey spectrum and C1s peak of carbonized silk fabric.
Fig. S4. *I-V* curves of carbonized silk fabric obtained at different temperatures.
Fig. S5. High-resolution XPS spectra of N1s for SilkNCT obtained at different temperatures.
Fig. S6. DPV responses of SilkNCT and C-cotton–based AA sensors to AA.
Fig. S7. Schematic diagram showing the working mechanisms of each sensor.
Fig. S8. SEM images of modified electrode for enzyme-based sensors.
Fig. S9. SEM images of modified electrode for ion-selective sensors.
Fig. S10. Sensing performance of the flexible SilkNCT-based electrochemical sensors for multiple biomarkers.
Fig. S11. Photographs of a sensing patch fabricated on a common silk fabric.
Fig. S12. Flexibility and stability of the SilkNCT-based flexible electrochemcial sensors.
Table S1. Atomic composition of pristine and carbonized silk fabric (obtained at 900°C).
Table S2. Gross content of N and relative content of various N species in SilkNCT samples obtained at different temperatures.
Table S3. Comparison of the sensitivity for various biomarkers of the recently reported wearable electrochemical sensors for sweat analysis with this work.
References (*41*–*48*)

REFERENCES AND NOTES

1. S. Choi, H. Lee, R. Ghaffari, T. Hyeon, D. H. Kim, Recent advances in flexible and stretchable bio-electronic devices integrated with nanomaterials. *Adv. Mater.* **28**, 4203–4218 (2016).
2. Y. Liu, M. Pharr, G. A. Salvatore, Lab-on-skin: A review of flexible and stretchable electronics for wearable health monitoring. *ACS Nano* **11**, 9614–9635 (2017).
3. X. Wang, Z. Liu, T. Zhang, Flexible sensing electronics for wearable/attachable health monitoring. *Small* **13**, 1602790 (2017).
4. Y. Yang, W. Gao, Wearable and flexible electronics for continuous molecular monitoring. *Chem. Soc. Rev.* **48**, 1465–1491 (2019).
5. S. Imani, A. J. Bandodkar, A. M. Mohan, R. Kumar, S. Yu, J. Wang, P. P. Mercier, A wearable chemical-electrophysiological hybrid biosensing system for real-time health and fitness monitoring. *Nat. Commun.* **7**, 11650 (2016).
6. Z. Sonner, E. Wilder, J. Heikenfeld, G. Kasting, F. Beyette, D. Swaile, F. Sherman, J. Joyce, J. Hagen, N. Kelley-Loughnane, R. Naik, The microfluidics of the eccrine sweat gland, including biomarker partitioning, transport, and biosensing implications. *Biomicrofluidics* **9**, 031301 (2015).
7. M. Bariya, H. Y. Y. Nyein, A. Javey, Wearable sweat sensors. *Nat. Electron.* **1**, 160–171 (2018).
8. A. Koh, D. Kang, Y. Xue, S. Lee, R. M. Pielak, J. K. Kim, T. Hwang, S. Min, A. Banks, P. Bastien, M. C. Manco, L. Wang, K. R. Ammann, K. Jang, P. Won, S. Han, R. Ghaffari, U. Paik, M. J. Slepian, G. Balooch, Y. Huang, J. A. Rogers, A soft, wearable microfluidic device for the capture, storage, and colorimetric sensing of sweat. *Sci. Transl. Med.* **8**, 366ra165 (2016).
9. N. Promphet, P. Rattanawaleedirojn, K. Siralertmukul, N. Soatthiyanon, P. Potiyaraj, C. Thanawattano, J. P. Hinestroza, N. Rodthongkum, Non-invasive textile based colorimetric sensor for the simultaneous detection of sweat pH and lactate. *Talanta* **192**, 424–430 (2019).
10. S. B. Kim, Y. Zhang, S. M. Won, A. J. Bandodkar, Y. Sekine, Y. Xue, J. Koo, S. W. Harshman, J. A. Martin, J. M. Park, T. R. Ray, K. E. Crawford, K. T. Lee, J. Choi, R. L. Pitsch, C. C. Grigsby, A. J. Strang, Y. Y. Chen, S. Xu, J. Kim, A. Koh, J. S. Ha, Y. Huang, S. W. Kim, J. A. Rogers, Super-absorbent polymer valves and colorimetric chemistries for time-sequenced discrete sampling and chloride analysis of sweat via skin-mounted soft microfluidics. *Small* **14**, e1703334 (2018).
11. Y. Chen, S. Lu, S. Zhang, Y. Li, Z. Qu, Y. Chen, B. Lu, X. Wang, X. Feng, Skin-like biosensor system via electrochemical channels for noninvasive blood glucose monitoring. *Sci. Adv.* **3**, e1701629 (2017).
12. X. Xuan, H. S. Yoon, J. Y. Park, A wearable electrochemical glucose sensor based on simple and low-cost fabrication supported micro-patterned reduced graphene oxide nanocomposite electrode on flexible substrate. *Biosens. Bioelectron.* **109**, 75–82 (2018).
13. L. Wang, L. Wang, Y. Zhang, J. Pan, S. Li, X. Sun, B. Zhang, H. Peng, Weaving sensing fibers into electrochemical fabric for real-time health monitoring. *Adv. Funct. Mater.* **28**, 1804456 (2018).
14. J. P. Kim, Z. Xie, M. Creer, Z. Liu, J. Yang, Citrate-based fluorescent materials for low-cost chloride sensing in the diagnosis of cystic fibrosis. *Chem. Sci.* **8**, 550–558 (2017).
15. X.-Y. Xu, B. Yan, A fluorescent wearable platform for sweat Cl^- analysis and logic smart-device fabrication based on color adjustable lanthanide MOFs. *J. Mater. Chem. C* **6**, 1863–1869 (2018).
16. Z. H. Jin, Y. L. Liu, J. J. Chen, S. L. Cai, J. Q. Xu, W. H. Huang, Conductive polymer-coated carbon nanotubes to construct stretchable and transparent electrochemical sensors. *Anal. Chem.* **89**, 2032–2038 (2017).
17. J. Kim, R. Kumar, A. J. Bandodkar, J. Wang, Advanced materials for printed wearable electrochemical devices: A review. *Adv. Electron. Mater.* **3**, 1600260 (2017).
18. Y. L. Liu, Y. Qin, Z. H. Jin, X. B. Hu, M. M. Chen, R. Liu, C. Amatore, W. H. Huang, A stretchable electrochemical sensor for inducing and monitoring cell mechanotransduction in real time. *Angew. Chem. Int. Ed.* **56**, 9454–9458 (2017).
19. A. J. Bandodkar, J. Wang, Non-invasive wearable electrochemical sensors: A review. *Trends Biotechnol.* **32**, 363–371 (2014).
20. S. Emaminejad, W. Gao, E. Wu, Z. A. Davies, H. Yin Yin Nyein, S. Challa, S. P. Ryan, H. M. Fahad, K. Chen, Z. Shahpar, S. Talebi, C. Milla, A. Javey, R. W. Davis, Autonomous sweat extraction and analysis applied to cystic fibrosis and glucose monitoring using a fully integrated wearable platform. *Proc. Natl. Acad. Sci. U.S.A.* **114**, 4625–4630 (2017).
21. Y. Wang, Y. Qiu, S. K. Ameri, H. Jang, Z. Dai, Y. Huang, N. Lu, Low-cost, μm-thick, tape-free electronic tattoo sensors with minimized motion and sweat artifacts. *npj Flex. Electron.* **2**, 6 (2018).
22. S. Wang, Y. Wu, Y. Gu, T. Li, H. Luo, L. H. Li, Y. Bai, L. Li, L. Liu, Y. Cao, H. Ding, T. Zhang, Wearable sweatband sensor platform based on gold nanodendrite array as efficient solid contact of ion-selective electrode. *Anal. Chem.* **89**, 10224–10231 (2017).
23. R. D. Munje, S. Muthukumar, S. Prasad, Lancet-free and label-free diagnostics of glucose in sweat using zinc oxide based flexible bioelectronics. *Sensor. Actuat. B Chem.* **238**, 482–490 (2017).
24. A. Bhide, S. Muthukumar, A. Saini, S. Prasad, Simultaneous lancet-free monitoring of alcohol and glucose from low-volumes of perspired human sweat. *Sci. Rep.* **8**, 6507 (2018).
25. H. Lee, T. K. Choi, Y. B. Lee, H. R. Cho, R. Ghaffari, L. Wang, H. J. Choi, T. D. Chung, N. Lu, T. Hyeon, S. H. Choi, D. H. Kim, A graphene-based electrochemical device with thermoresponsive microneedles for diabetes monitoring and therapy. *Nat. Nanotechnol.* **11**, 566–572 (2016).
26. Z. Wang, S. Dong, M. Gui, M. Asif, W. Wang, F. Wang, H. Liu, Graphene paper supported MoS_2 nanocrystals monolayer with Cu submicron-buds: High-performance flexible platform for sensing in sweat. *Anal. Biochem.* **543**, 82–89 (2018).
27. T. Glennon, C. O'Quigley, M. McCaul, G. Matzeu, S. Beirne, G. G. Wallace, F. Stroiescu, N. O'Mahoney, P. White, D. Diamond, 'SWEATCH': A wearable platform for harvesting and analysing sweat sodium content. *Electroanalysis* **28**, 1283–1289 (2016).
28. H. Tao, D. L. Kaplan, F. G. Omenetto, Silk materials—A road to sustainable high technology. *Adv. Mater.* **24**, 2824–2837 (2012).
29. Z. Zhou, S. Zhang, Y. Cao, B. Marelli, X. Xia, T. H. Tao, Engineering the future of silk materials through advanced manufacturing. *Adv. Mater.* **30**, 1706983 (2018).
30. S. Y. Cho, Y. S. Yun, S. Lee, D. Jang, K. Y. Park, J. K. Kim, B. H. Kim, K. Kang, D. L. Kaplan, H. J. Jin, Carbonization of a stable β-sheet-rich silk protein into a pseudographitic pyroprotein. *Nat. Commun.* **6**, 7145 (2015).
31. C. Wang, X. Li, E. Gao, M. Jian, K. Xia, Q. Wang, Z. Xu, T. Ren, Y. Zhang, Carbonized silk fabric for ultrastretchable, highly sensitive, and wearable strain sensors. *Adv. Mater.* **28**, 6640–6648 (2016).
32. C. Wang, K. Xia, M. Jian, H. Wang, M. Zhang, Y. Zhang, Carbonized silk georgette as an ultrasensitive wearable strain sensor for full-range human activity monitoring. *J. Mater. Chem. C* **5**, 7604–7611 (2017).

33. Q. Wang, M. Jian, C. Wang, Y. Zhang, Carbonized silk nanofiber membrane for transparent and sensitive electronic skin. *Adv. Funct. Mater.* **27**, 1605657 (2017).
34. C. Wang, N.-H. Xie, Y. Zhang, Z. Huang, K. Xia, H. Wang, S. Guo, B.-Q. Xu, Y. Zhang, Silk-derived highly active oxygen electrocatalysts for flexible and rechargeable Zn–Air batteries. *Chem. Mater.* **31**, 1023–1029 (2019).
35. C. Wang, W. Chen, K. Xia, N. Xie, H. Wang, Y. Zhang, Silk-derived 2D porous carbon nanosheets with atomically-dispersed Fe-N_x -C sites for highly efficient oxygen reaction catalysts. *Small* **15**, 1804966 (2019).
36. S. B. Yoon, G. S. Chai, S. K. Kang, J.-S. Yu, K. P. Gierszal, M. Jaroniec, Graphitized pitch-based carbons with ordered nanopores synthesized by using colloidal crystals as templates. *J. Am. Chem. Soc.* **127**, 4188–4189 (2005).
37. S. H. Lim, R. Li, W. Ji, J. Lin, Effects of nitrogenation on single-walled carbon nanotubes within density functional theory. *Phys. Rev. B* **76**, 195406 (2007).
38. W. He, C. Jiang, J. Wang, L. Lu, High-rate oxygen electroreduction over graphitic-N species exposed on 3D hierarchically porous nitrogen-doped carbons. *Angew. Chem. Int. Ed.* **53**, 9503–9507 (2014).
39. L. He, F. Weniger, H. Neumann, M. Beller, Synthesis, characterization, and application of metal nanoparticles supported on nitrogen-doped carbon: Catalysis beyond electrochemistry. *Angew. Chem. Int. Ed.* **55**, 12582–12594 (2016).
40. W. Gao, S. Emaminejad, H. Y. Y. Nyein, S. Challa, K. Chen, A. Peck, H. M. Fahad, H. Ota, H. Shiraki, D. Kiriya, D. H. Lien, G. A. Brooks, R. W. Davis, A. Javey, Fully integrated wearable sensor arrays for multiplexed in situ perspiration analysis. *Nature* **529**, 509–514 (2016).
41. J. R. Sempionatto, T. Nakagawa, A. Pavinatto, S. T. Mensah, S. Imani, P. Mercier, J. Wang, Eyeglasses based wireless electrolyte and metabolite sensor platform. *Lab Chip* **17**, 1834–1842 (2017).
42. G. Xu, C. Cheng, Z. Liu, W. Yuan, X. Wu, Y. Lu, S. S. Low, J. Liu, L. Zhu, D. Ji, S. Li, Z. Chen, L. Wang, Q. Yang, Z. Cui, Q. Liu, Battery-free and wireless epidermal electrochemical system with all-printed stretchable electrode array for multiplexed in situ sweat analysis. *Adv. Mater. Technol.* **4**, 1800658 (2019).
43. A. Martin, J. Kim, J. F. Kurniawan, J. R. Sempionatto, J. R. Moreto, G. Tang, A. S. Campbell, A. Shin, M. Y. Lee, X. Liu, J. Wang, Epidermal microfluidic electrochemical detection system: Enhanced sweat sampling and metabolite detection. *ACS Sensors* **2**, 1860–1868 (2017).
44. L. Lipani, B. G. R. Dupont, F. Doungmene, F. Marken, R. M. Tyrrell, R. H. Guy, A. Ilie, Non-invasive, transdermal, path-selective and specific glucose monitoring via a graphene-based platform. *Nat. Nanotechnol.* **13**, 504–511 (2018).
45. S. Y. Oh, S. Y. Hong, Y. R. Jeong, J. Yun, H. Park, S. W. Jin, G. Lee, J. H. Oh, H. Lee, S. S. Lee, J. S. Ha, Skin-attachable, stretchable electrochemical sweat sensor for glucose and pH detection. *ACS Appl. Mater. Inter.* **10**, 13729–13740 (2018).
46. W. Jia, A. J. Bandodkar, G. Valdes-Ramirez, J. R. Windmiller, Z. Yang, J. Ramirez, G. Chan, J. Wang, Electrochemical tattoo biosensors for real-time noninvasive lactate monitoring in human perspiration. *Anal. Chem.* **85**, 6553–6560 (2013).
47. H. Y. Y. Nyein, L. C. Tai, Q. P. Ngo, M. Chao, G. B. Zhang, W. Gao, M. Bariya, J. Bullock, H. Kim, H. M. Fahad, A. Javey, A wearable microfluidic sensing patch for dynamic sweat secretion analysis. *ACS Sensors* **3**, 944–952 (2018).
48. M. McCaul, A. Porter, R. Barrett, P. White, F. Stroiescu, G. Wallace, D. Diamond, Wearable platform for real-time monitoring of sodium in sweat. *ChemPhysChem* **19**, 1531–1536 (2018).

Acknowledgments

Funding: We acknowledge the support from the National Natural Science Foundation of China (51672153), the National Key Basic Research and Development Program (2016YFA0200103), and the National Program for Support of Top-Notch Young Professionals.

Author contributions: Y.Z. and W.H. proposed the concept and designed the experiment. W.H. carried out most of the experiment with the help from other co-authors. C.W., M.J., and W.L. participated in the fabrication and electrochemical characterization of the sensors. H.W. and X.L. provided support for the on-body trial of device. F.Y. and X.Z. provided technical guidance for electrochemical analysis. W.H. and Y.Z. wrote the paper with inputs from all the others. All authors discussed the results and contributed to proofreading the manuscript.
Competing interests: The authors declare that they have no competing interests. **Data and materials availability:** All data needed to evaluate the conclusions in the paper are present in the paper and/or the Supplementary Materials. Additional data related to this paper may be requested from the authors.

Submitted 19 March 2019
Accepted 17 September 2019
Published 8 November 2019
10.1126/sciadv.aax0649

Citation: W. He, C. Wang, H. Wang, M. Jian, W. Lu, X. Liang, X. Zhang, F. Yang, Y. Zhang, Integrated textile sensor patch for real-time and multiplex sweat analysis. *Sci. Adv.* **5**, eaax0649 (2019).